

SUPPORTING INFORMATION

Does Boron or Nitrogen Substitution Affect Hydrogen Physisorption on Open Carbon Surfaces?

Rylan Rowsey,¹ Erin E. Taylor,¹ Ryan W. Hinson,¹ Dalton Compton,¹ Nicholas P. Stadie,^{1*} and Robert K. Szilagyi^{2*}

¹ Department of Chemistry & Biochemistry, Montana State University, Bozeman, MT 59717, U.S.A.

² Department of Chemistry, The University of British Columbia – Okanagan, Kelowna, BC V1V 1V7, Canada

*Corresponding authors: nstadie@montana.edu and robert.szilagyi@ubc.ca.

Table of Contents

Table S1:	Literature survey of experimental H ₂ isosteric heat of physisorption on carbon surfaces (ΔH_{ads} , kJ mol ⁻¹)	5
Table S2:	Literature survey of theoretical H ₂ binding energies (physisorption) on carbon surfaces (ΔE_{ads} , kJ mol ⁻¹).....	6
Computational Models		7
Scheme S1:	Graphical illustrations of the nomenclature employed for representative internal coordinates of the adsorbent. The “inner”, “outer”, and “peripheral” positions are defined by the αC , βC , and γC atoms, and the methylenic $\gamma'\text{C}$ atom, respectively. The planarity of the molecule and the wagging character of the methylenic group are described by the distance (δ) between the site of substitution (X_1) and the plane formed by the ring centroids (X_{I} , X_{II} , and X_{III}) and by the angle (w) between the $\gamma'\text{C}\cdots ipso\text{-}\beta\text{C}\cdots para\text{-}\alpha\text{C}$ of ring I, respectively.....	7

Table S3:	Z-matrix definitions for the end-on (κ_1) and the side-on (η^2) approaches of H_2 to the MPh adsorbent model (above Ring I containing the methylene group).	8
Scheme S2:	Graphical illustration of all the 35 configurations of H_2 interactions with the MPh adsorbate considered in this study.	9
Figure S1:	Potential energy surface maps for H_2 adsorbate interaction with the MPh adsorbent and its B- and N-substituted derivatives. Initial structures for higher-level calculations were selected from approximately middle of the potential surface maps ($X1...H = \sim 2.0 \text{ \AA}$ adsorbate/adsorbent distance and $\sim 130^\circ X1...H-H$ angle, where X1 is the central atom in the MPh adsorbate structure).	13
Figure S2:	Structures from PES scans (Figure S1) selected for generating the initial 3×3 set of structures to be refined at higher levels of theory.	14
Table S4.	Adsorption model structures (Level of Theory, LoT: MN15/6-311++G**) of H_2 on MPh, B-MPh, or N-MPh (averages and standard deviations of inner (α), outer (β), and peripheral (γ) sphere C-C distances in \AA , out-of-plane distortion (δ , \AA) of the site of substitution, and methylene group wagging angle (ω , $^\circ$) of the methylene group) with one ($n = 1$), two ($n = 2$, opposite face, superscripts indicate occupied rings with adsorbate), and six ($n = 6$, model saturation) adsorbate molecules described by H_2 bond centroid (X_{H_2}) and nearest ring centroid (X_i) distances (d_i , \AA where i subscript represents ring I, II, or III H_2 is located above), H_2 angle of approach defined by ring centroid(X_i)... $H-H$ (φ , $^\circ$) ranging from end-on ($\varphi = 180^\circ$) to side-on ($\varphi = 90^\circ$) orientation, tilt with respect to the site of substitution (X1) defined by $X1$...ring centroid...proximal H (ϕ , $^\circ$) bond angles, degree of deviation from centeredness of the $H-H$ bond centroid projections to the plane of the ring centroids from the nearest ring centroid (λ , \AA), and $H-H$ bond lengths of the adsorbed H_2 molecule.	15
Figure S3:	Estimated adsorption energies with BSSE and zero-point energy corrections according to $\Delta E^{QM^*} + \Delta E_{ZPE} + \Delta(PV)$ at MN15/6-311++G** level of theory) for all models shown in Scheme S2 . The dashed lines for the $n = 6$ adsorption models indicate structural isomers obtained by permuting the identity of the central site of substitution, X1, in the X-MPh model from the lowest energy structures represented by the solid lines. The permutation of composition was carried out in order to address potential pitfalls of comparing local as opposed to global potential energy surface minima. All of these permuted structures are higher in energy by at least more than 2.3, 0.1, and 0.7 kJ mol^{-1} for $X = B, C,$ and N when using $X = (C \text{ or } N), (B \text{ or } N),$ and $(B \text{ or } C)$ compositions, respectively.	16

Figure S4:	Level of theory dependence of MPh adsorbent/H ₂ adsorbate interaction energies for (Panel A) and Boltzmann weighed dissociation energies at standard state using $\Delta(E^{QM*}+E_{ZPE}+\Delta(PV))$ formalism from MN15/6-311++G** calculations as a function of surface coverage ($n = 1-6$) for X-MPh $\times nH_2$ (X = C shown as black circles, X = B as pink triangles, and X = N as blue squares) physisorption models (Panel B; the italicized numbers above data points correspond to average q_{st} values in kJ mol ⁻¹ per H ₂ molecule; the overall per H ₂ heat of adsorption was estimated to be 4.1±0.7 kJ mol ⁻¹).	17
Figure S5:	Comparison of optimized models at MN15/6-311++G** level of theory considering perbenzannulated MPh models (X-pbaMPh, X = C, B, or N) with key structural parameters (d_i and ϕ) describing the H ₂ interactions.....	18
Figure S6:	Two views of high H ₂ loading adsorption models optimized at MN15/6-311++G** level of theory using the X-pbaMPh adsorbent with 24 adsorbate molecules (top row) and curved blade models (middle and bottom rows) corresponding to low density (15 mol dm ⁻³ ; 30 adsorbates, middle row) and high density (38 mol dm ⁻³ ; 84 adsorbates, bottom row) liquid H ₂ environments. The top two models started from approximately co-linear, end-on H ₂ arrangements perpendicular to the closed ring with a 2.7 Å ring-centroid-to-proximal H distances, while the lower model was created by soaking the curve blade in liquid H ₂	19
Table S5:	Dissociation energies (in kJ mol ⁻¹) for (adsorbent) $\times nH_2 \rightarrow$ adsorbent + $n H_2$ reactions obtained from MN15/6-311++G** calculations. BSSE stands for basis set superposition error (in kJ mol ⁻¹). The structures of the extended models are shown in Figures S5-S6 . ΔH_{ads} or q_{st} is calculated by using $\Delta E^{QM*} + \Delta E_{ZPE} + \Delta PV$ (see Figure S8). Interaction energies (ΔE^{QM*}) among the adsorbates are -16 and -139 kJ mol ⁻¹ for 6 and 30 H ₂ molecules or -2.6 and -4.6 kJ mol ⁻¹ per molecule, respectively. B ₃ and N ₃ prefixes correspond to triple heteroatom substituted models, where the site of substitutions are separated by at least three C atoms.	20
Figure S7.	Experimental adsorption isotherms of H ₂ on ZTC at 77–298 K, fitted to three models to determine the experimental heat of H ₂ adsorption (ΔH_{exp} or q_{st}).	21
Table S6.	Best fit values for parameters that describe H ₂ adsorption on ZTC at 77–298 K within the framework of a dual-site Langmuir model (DL in Figure S8).....	21

Figure S8. Experimental isosteric heat of H₂ adsorption on ZTC (ΔH_{exp} or q_{st}) as a function of H₂ loading at room temperature, compared to various calculated quantities. USM stands for the thermal energy correction to the internal energy from statistical mechanics. The computationally-derived quantity that most closely matches experiment is the same as in previous work [Ref. 30]: $\Delta H_{\text{ads}} \approx \Delta E^{\text{QM}^*} + \Delta E_{\text{ZPE}} + \Delta PV$. Squares represent energies and diamonds represent enthalpies. The width of the transparent regions represents the uncertainty inherent to the experimental method. SL, DL, and UL stand for single-site, double-site, and uniform (“Unilan”) Langmuir models, respectively.....23

Atomic positional coordinates, electron density cube files, and other significant details of the computational studies are also provided at a Zenodo depository DOI: 10.5281/zenodo.4330760.

Table S1: Literature survey of experimental H₂ isosteric heat of physisorption on carbon surfaces (ΔH_{ads} , kJ mol⁻¹)

Undoped carbon surface

Author	Year	DOI	Material	ΔH_{ads}
Zhao	2005	10.1021/jp050080z	Activated Carbon	3.9-5.2
Nishihara	2009	10.1021/jp808890x	MSC-30	7.3
Nishihara	2009	10.1021/jp808890x	ZTC	8
Xia	2009	10.1021/ja9054838	ZTC	~8
Stadie	2012	10.1021/la302050m	CNS-201	8.6
Stadie	2012	10.1021/la302050m	MSC-30	6.7
Stadie	2012	10.1021/la302050m	ZTC	6.5-6.6
Shcherban	2017	10.1007/s10853-016-0447-x	CMK-3	4.9

B-doped carbon surface

Author	Year	DOI	Material	ΔH_{ads}
Chung	2008	10.1021/ja800071y	Microporous Carbon	12.47
Jin	2010	10.1021/ja105428d	Carbon Scaffold	8.6
Kleinhammes	2010	10.1021/jp102972c	Graphitic Carbon	11.4
Jeong	2010	10.1016/j.carbon.2010.03.029	Activated Carbon	12-20
Shcherban	2017	10.1007/s10853-016-0447-x	CMK-3	5.1

N-doped carbon surface

Author	Year	DOI	Material	ΔH_{ads}
Xia	2009	10.1021/ja9054838	ZTC	~8
Jin	2010	10.1021/ja105428d	Carbon Scaffold	5.6
Ariharan	2017	10.4236/graphene.2017.62004	Few-Layer Graphite	N/D
Blankenship	2017	10.1039/C7EE02616A	Hydrochar	N/D

Table S2: Literature survey of theoretical H₂ binding energies (physisorption) on carbon surfaces (ΔE_{ads} , kJ mol⁻¹)

Undoped carbon surface

Author	Year	DOI	Material	Method	ΔE_{ads}
Varenius	2011	fulltext/152983.pdf	graphene coronene	GGA	5.7-6.9
Nayyar	2020	10.3390/c6010015	coronene	B3LYP	6.2
Yeamin	2014	10.1039/C4RA08487J	coronene	B3LYP	9.43
Firlej	2009	10.1063/1.3251788	pyrene	MP2+GCMC	5.6
Zhou	2006	10.1016/j.carbon.2005.10.016	single wall nanotube	GGA	1.80-10.33

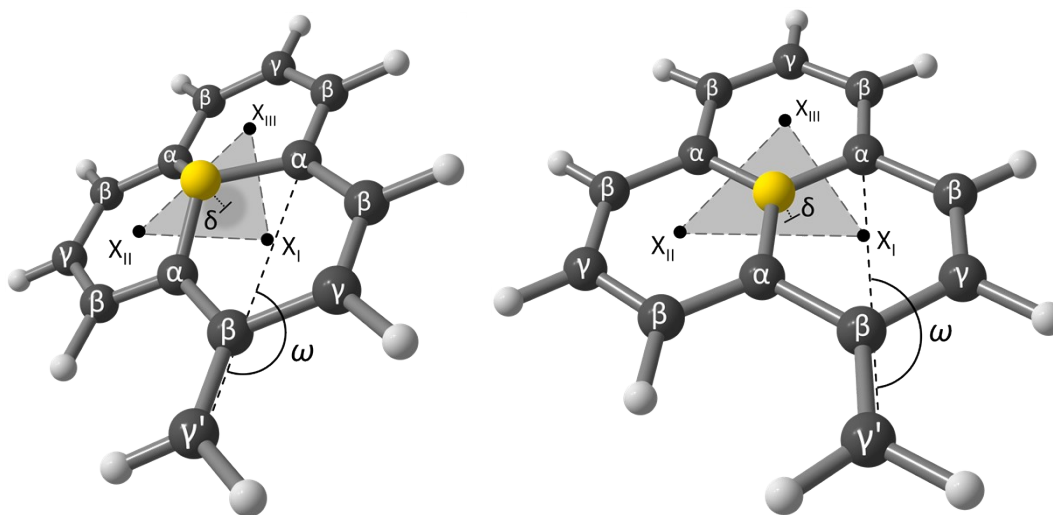
B-doped carbon surface

Author	Year	DOI	Material	Method	ΔE_{ads}
Dai	2009	10.1063/1.3272008	graphene	GGA	1.35
Nayyar	2020	10.3390/c6010015	coronene	B3LYP	5.6-7.6
Firlej	2009	10.1063/1.3251788	pyrene	MP2+GCMC	7.8
Zhou	2006	10.1016/j.carbon.2005.10.016	single wall nanotube	GGA	0.71-3.60

N-doped carbon surface

Author	Year	DOI	Material	Method	ΔE_{ads}
Dai	2009	10.1063/1.3272008	graphene	GGA	0.77
Zhou	2006	10.1016/j.carbon.2005.10.016	single wall nanotube	GGA	0.04-6.15

Computational Models



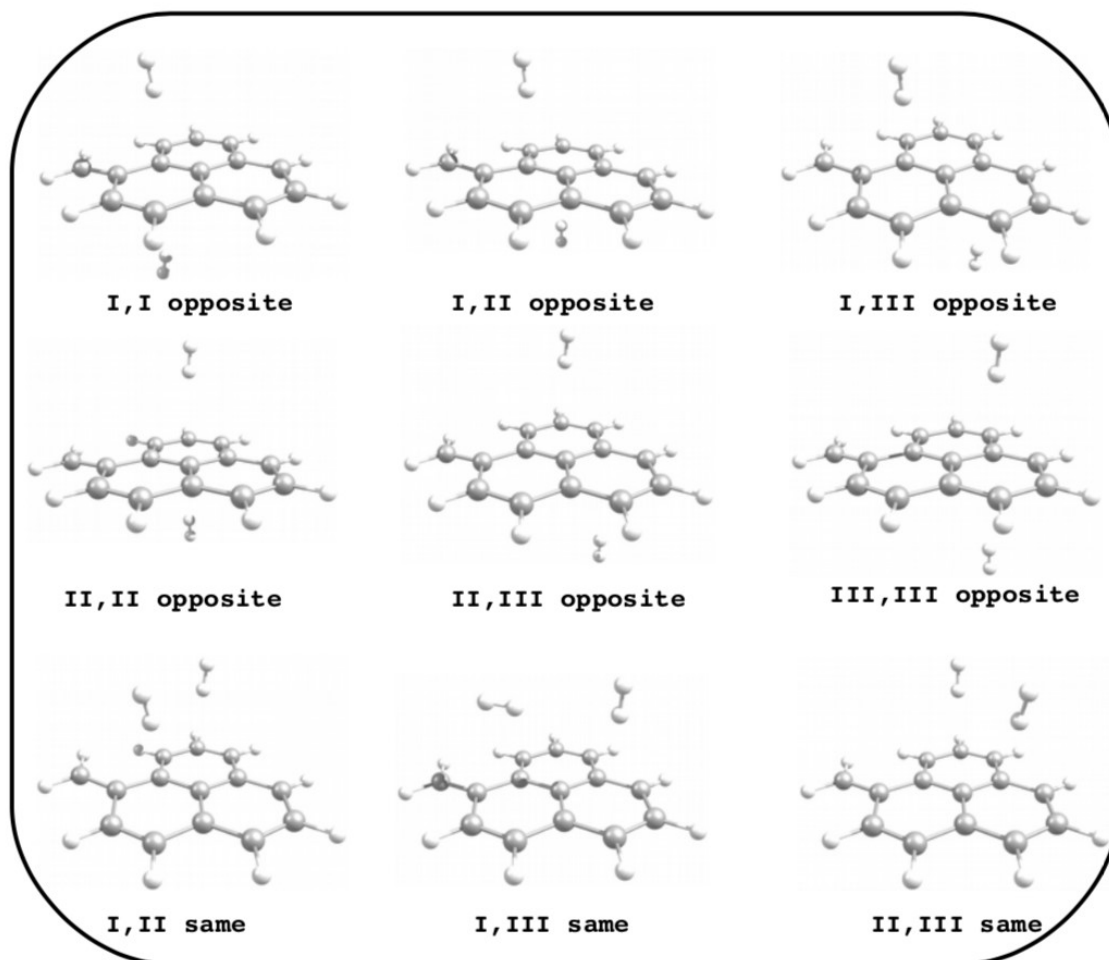
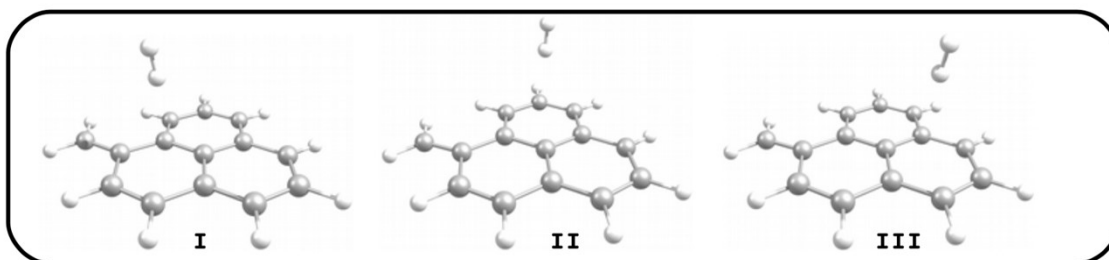
Scheme S1: Graphical illustrations of the nomenclature employed for representative internal coordinates of the adsorbent. The “inner”, “outer”, and “peripheral” positions are defined by the α C, β C, and γ C atoms, and the methylene γ' C atom, respectively. The planarity of the molecule and the wagging character of the methylene group are described by the distance (δ) between the site of substitution (X_I) and the plane formed by the ring centroids (X_I , X_{II} , and X_{III}) and by the angle (ω) between the γ' C \cdots *ipso*- β C \cdots *para*- α C of ring I, respectively.

The same levels of theory and general computational methodologies as employed in our recent methane adsorption study [Ref. 30] were also employed herein, based on the methylene phenalene (MPh) adsorbent model and its N- and B-substituted derivatives (B-MPh, N-MPh). Substitution is realized at the central (X_I) position with respect to the phenalene rings, with a methylene group appended to ensure extended π conjugation and the closed shell, singlet ground state of the unsubstituted model. This model can be used to investigate up to six H_2 adsorption interactions simultaneously, allowing for a much richer exploration of the landscape of adsorbent/adsorbate and adsorbate/adsorbate interactions than for methane (whose size permitted only up to two simultaneous interactions). In addition, we briefly considered expanded adsorbent models with various H_2 loading that included a perbenzannulated MPh model and a curved blade maquette directly taken out of a zeolite templated carbon model [Ref. 10]. The key difference between the H_2 and CH_4 adsorption is the preferred sites of adsorption, which is above ring centroids for H_2 and above the central graphitic site (X_I) for CH_4 . Another key difference for H_2 adsorption is the possibility to form either end-on (κ_1) or side-on (η^2) interactions above MPh, where for CH_4 all stable adsorption models showed the same “lander” geometry described in detail in that work. The internal coordinates of the end-on and side-on models used for the initial potential energy surface mapping are shown in **Table S3**.

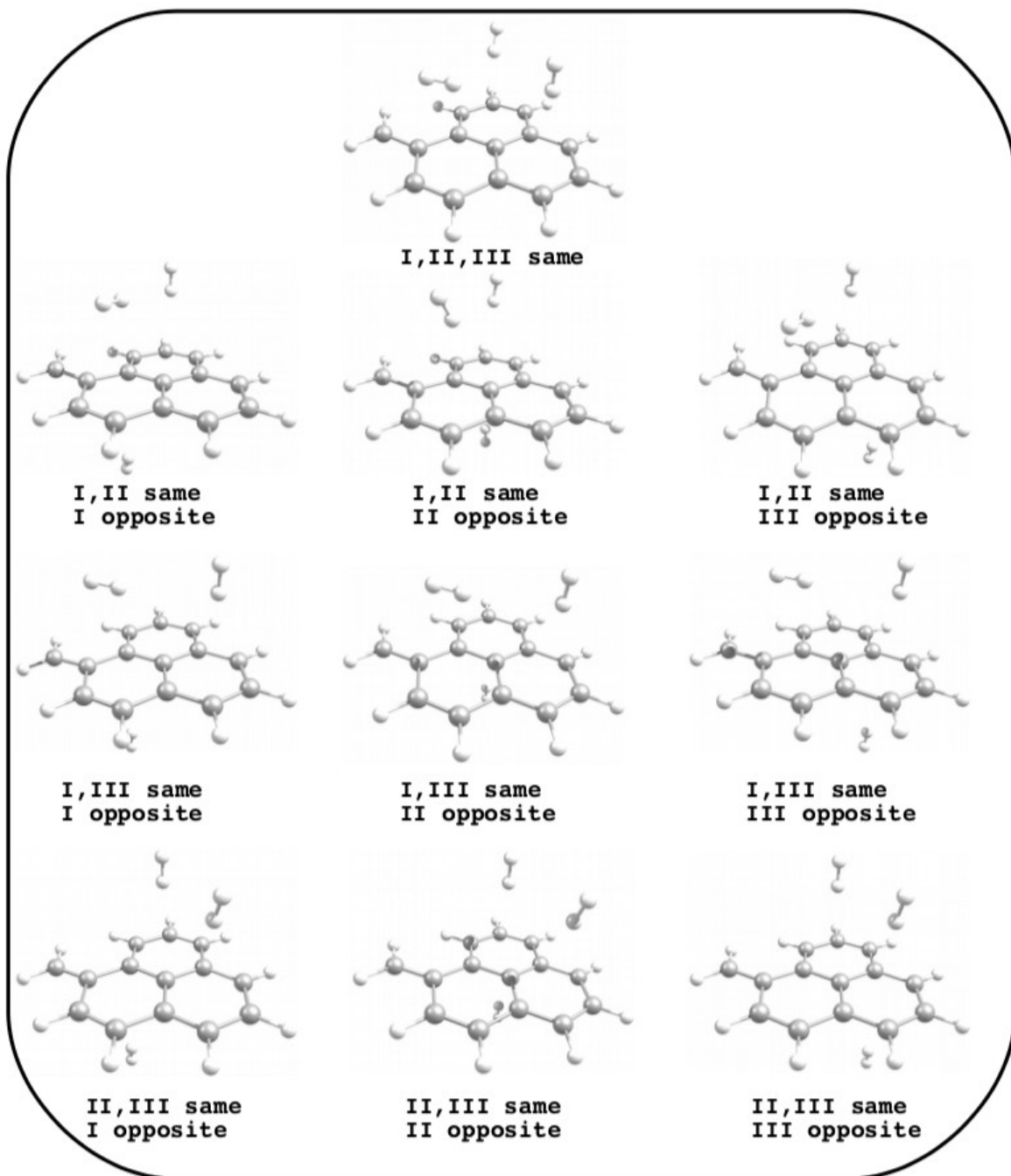
Table S3: Z-matrix definitions for the end-on (κ_1) and the side-on (η^2) approaches of H₂ to the MPh adsorbent model (above Ring I containing the methyldene group).

κ_1 -H ₂	η^2 -H ₂
E/C/N	E/C/N
X 1 rXC	X 1 rXC
H 2 rHX 1 qHaXC	H 2 rHX 1 qHaXC
H 3 rHH 2 qHHX 1 wHHXC	H 3 rHH 2 qHHX 1 wHHXC
C 1 rCaC 2 qCaCX 3 wCaaCXH	C 1 rCaC 2 qCaCX 3 wCaaCXH
C 1 rCaC 2 qCaCX 3 -wCaaCXH	C 1 rCaC 2 qCaCX 3 -wCaaCXH
C 1 rCaC 2 qCaCX 3 wCabCXH	C 1 rCaC 2 qCaCX 3 wCabCXH
C 5 rCbCa 1 qCbCaC 2 -wCbCaCX	C 5 rCbCa 1 qCbCaC 2 -wCbCaCX
C 5 rCbCa 1 qCbCaC 2 wCbCaCX	C 5 rCbCa 1 qCbCaC 2 wCbCaCX
C 6 rCbCa 1 qCbCaC 2 wCbCaCX	C 6 rCbCa 1 qCbCaC 2 wCbCaCX
C 6 rCbCa 1 qCbCaC 2 -wCbCaCX	C 6 rCbCa 1 qCbCaC 2 -wCbCaCX
C 7 rCbCa 1 qCbCaC 2 -wCbCaCX	C 7 rCbCa 1 qCbCaC 2 -wCbCaCX
C 7 rCbCa 1 qCbCaC 2 wCbCaCX	C 7 rCbCa 1 qCbCaC 2 wCbCaCX
C 8 rCmCb 5 qCmCbCa 1 wCmCbCaC	C 8 rCmCb 5 qCmCbCa 1 wCmCbCaC
H 14 rHCm 8 qHCmCb 5 wHCmCbCa	H 14 rHCm 8 qHCmCb 5 wHCmCbCa
H 14 rHCm 8 qHCmCb 15 wHCmCbH	H 14 rHCm 8 qHCmCb 15 wHCmCbH
C 8 rCcCb 5 qCcCbCa 1 wCcCbCaC	C 8 rCcCb 5 qCcCbCa 1 wCcCbCaC
H 17 rHCc 8 qHCcCb 5 wHCcCbCa	H 17 rHCc 8 qHCcCb 5 wHCcCbCa
C 9 rCcCb 5 qCcCbCa 1 wCcCbCaC	C 9 rCcCb 5 qCcCbCa 1 wCcCbCaC
H 19 rHCc 9 qHCcCb 5 wHCcCbCa	H 19 rHCc 9 qHCcCb 5 wHCcCbCa
C 11 rCcCb 6 qCcCbCa 1 wCcCbCaC	C 11 rCcCb 6 qCcCbCa 1 wCcCbCaC
H 21 rHCc 11 qHCcCb 6 wHCcCbCa	H 21 rHCc 11 qHCcCb 6 wHCcCbCa
H 9 rHCb 5 qHCbCa 1 wHCbCaC	H 9 rHCb 5 qHCbCa 1 wHCbCaC
H 10 rHCb 6 qHCbCa 1 wHCbCaC	H 10 rHCb 6 qHCbCa 1 wHCbCaC
H 11 rHCb 6 qHCbCa 1 wHCbCaC	H 11 rHCb 6 qHCbCa 1 wHCbCaC
H 12 rHCb 7 qHCbCa 1 wHCbCaC	H 12 rHCb 7 qHCbCa 1 wHCbCaC
H 13 rHCb 7 qHCbCa 1 wHCbCaC	H 13 rHCb 7 qHCbCa 1 wHCbCaC
rXC 3.0 8 -0.25	rXC 3.0 8 -0.25
rHX 0.395	rHX 0.395
rHH 0.79	rHH 0.79
qHaXC 89.9 8 -11.1	qHaXC 89.9 8 -11.1
qHHX 0.0	qHHX 0.0
wHHXC 90.0	wHHXC 90.0
rCaC 1.435	rCaC 1.435
qCaCX 90.0	qCaCX 90.0
wCaaCXH 60.0	wCaaCXH 60.0
wCabCXH 180.0	wCabCXH 180.0
rCbCa 1.435	rCbCa 1.435
qCbCaC 120.0	qCbCaC 120.0
wCbCaCX 90.0	wCbCaCX 90.0
rCmCb 1.36	rCmCb 1.36
qCmCbCa 120.0	qCmCbCa 120.0
wCmCbCaC 180.0	wCmCbCaC 180.0
rHCm 1.09	rHCm 1.09
qHCmCb 120.0	qHCmCb 120.0
wHCmCbCa 180.0	wHCmCbCa 180.0
wHCmCbH 180.0	wHCmCbH 180.0
rCcCb 1.435	rCcCb 1.435
qCcCbCa 120.0	qCcCbCa 120.0
wCcCbCaC 0.0	wCcCbCaC 0.0
rHCc 1.09	rHCc 1.09
qHCcCb 120.0	qHCcCb 120.0
wHCcCbCa 180.0	wHCcCbCa 180.0
rHCb 1.09	rHCb 1.09
qHCbCa 120.0	qHCbCa 120.0
wHCbCaC 180.0	wHCbCaC 180.0

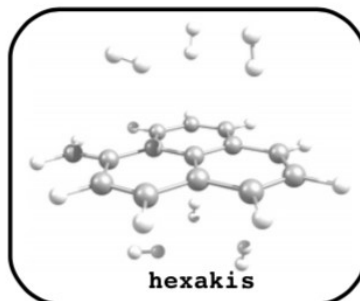
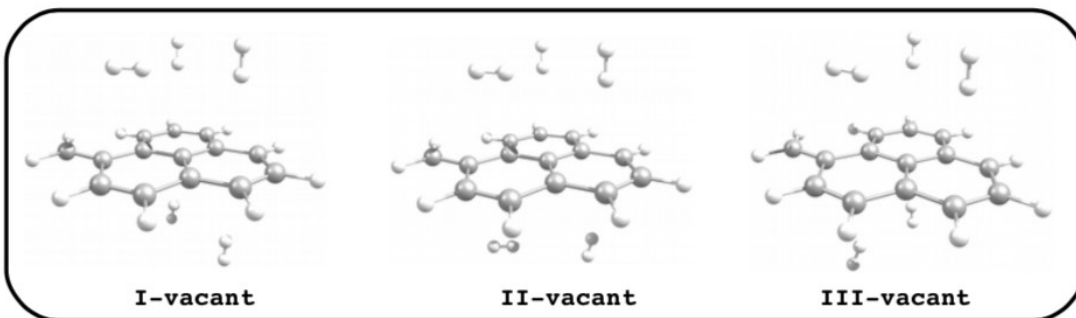
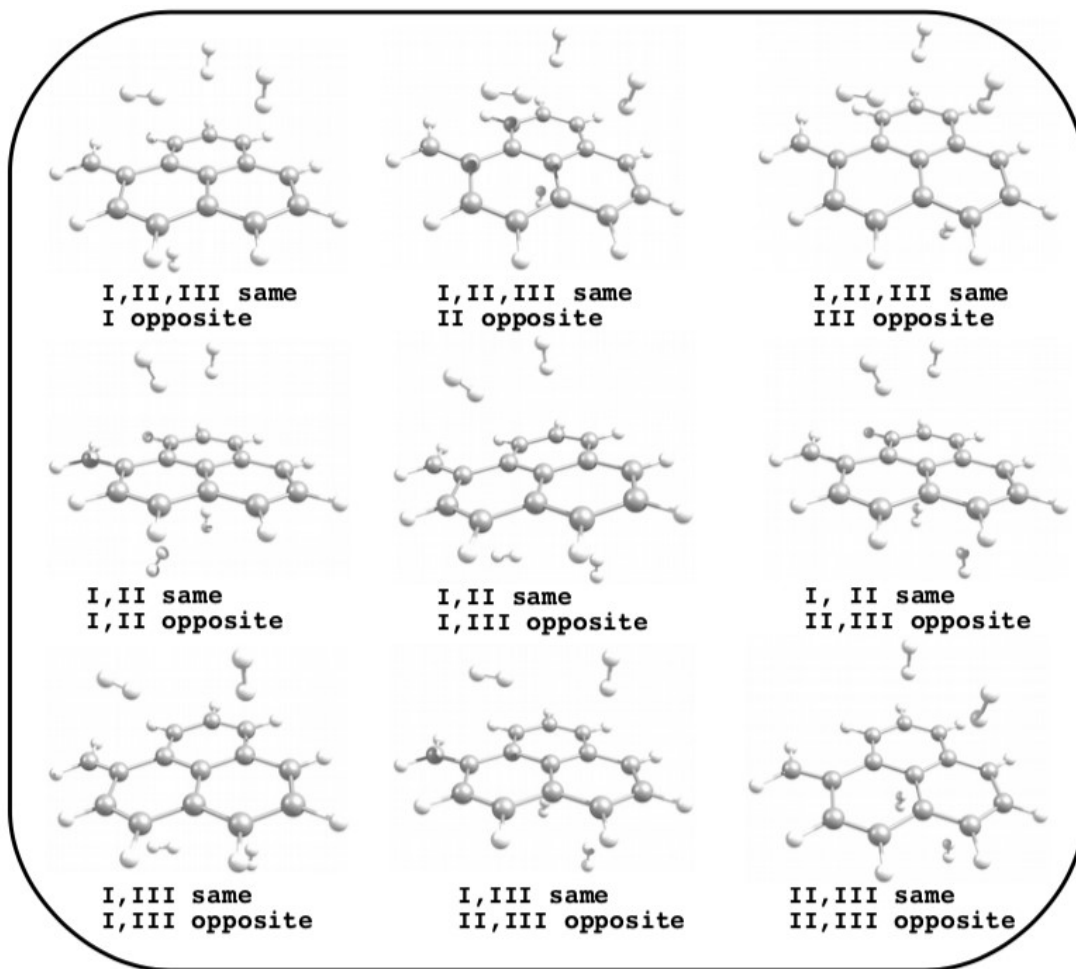
The Z-matrix definitions in **Table S3** permitted the systematic mapping of all 35 possible arrangements of up to 6 H₂ molecules on both sides of the MPh adsorbent, as graphically summarized in **Scheme S2**. These arrangements emerge from considering the number of H₂ molecules distributed among the three unique rings of the MPh adsorbent with slightly different chemical environments due to the presence of the methyldene group (**Figure 1**).



Scheme S2: Graphical illustration of all the 35 configurations of H₂ interactions with the MPh adsorbate considered in this study.



Scheme S2: (continued).



Scheme S2: (continued).

As in previous work [Ref. 30], the initial structures for H₂ adsorption models were generated from potential energy surface (PES) maps (**Figure S1**) as a function of the adsorbate distance and orientation relative to the site of substitution of MPh. The H₂ adsorbate geometry was described in both side-on (μ^2) and end-on (μ^1) approaches (**Table S3**). The PBE/6-311++G** level of theory was utilized for mapping the PES without employing empirical dispersion correction in order to obtain well-defined and structurally different local minima as a function of heteroatom substitution. As **Figure S1** summarizes, there were only minor differences in the overall PES curvature among the MPh×H₂, B-MPh×H₂, and N-MPh×H₂ adsorption models. A difference was observed at short distances ($X1...H^p < 1.2 \text{ \AA}$) for the unsubstituted and N-containing models, a part of the PES more characteristic of chemisorption (H–H bond breaking, H₂ ionization to hydride and proton) outside of the present focus on physisorption dominated by non-covalent interactions.

Using internal coordinates (**Table S3**), the H₂ molecule was driven toward the central site (X1); in all cases, the adsorbate slipped into one of various local minima above one of the rings of the MPh adsorbent (**Figure S2**). We took advantage of the resulting structural diversity and created a 3×3 initial set of structures for analyses at higher levels of theory by permuting the nature of the graphitic site (X1 = C, B, or N) and the orientation of the H₂ molecule. Upon refinement of these initial structures at either the reference level of DFT, MN15/6-311++G** (“MN15”), or corresponding level of correlated MO theory, MP2/6-311++G** (“MP2”), the nine initial structures converged to three different optimized structures with H₂ molecules above one of the three rings.

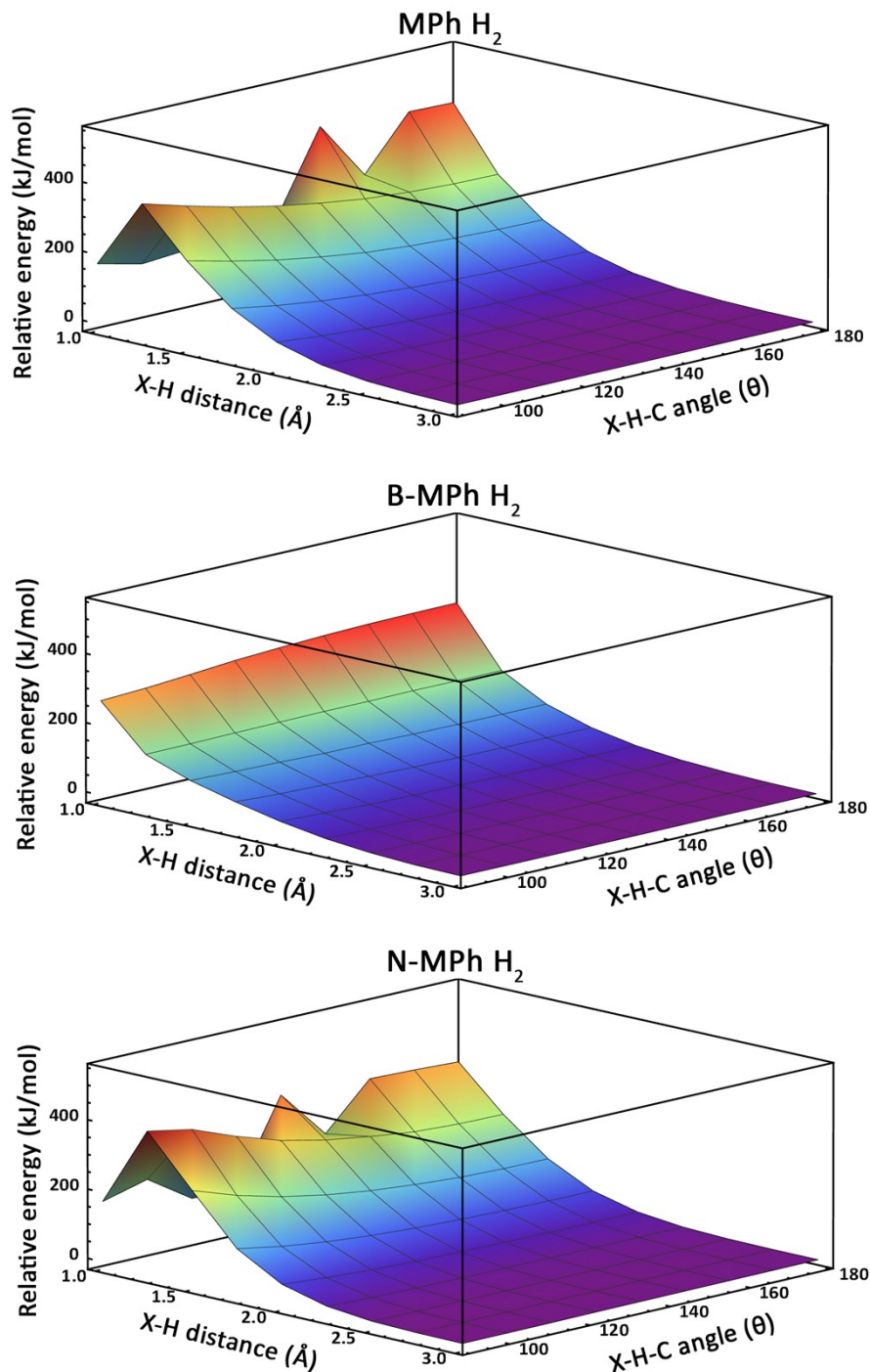


Figure S1: Potential energy surface maps for H₂ adsorbate interaction with the MPh adsorbent and its B- and N-substituted derivatives. Initial structures for higher-level calculations were selected from approximately middle of the potential surface maps (X1...H = ~2.0 Å adsorbate/adsorbent distance and ~130° X1...H-H angle, where X1 is the central atom in the MPh adsorbate structure).

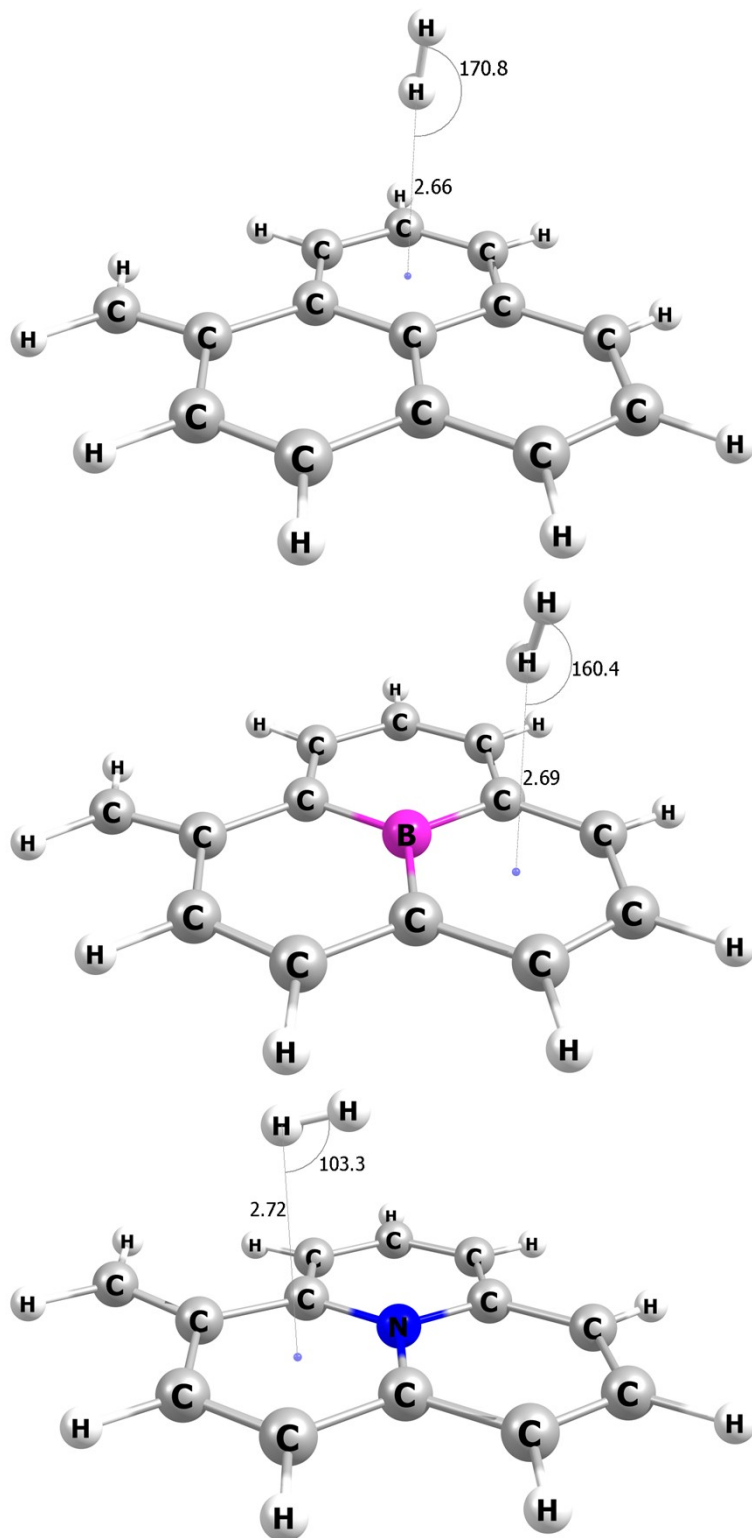


Figure S2: Structures from PES scans (Figure S1) selected for generating the initial 3×3 set of structures to be refined at higher levels of theory.

Table S4. Adsorption model structures (Level of Theory, LoT: MN15/6-311++G**) of H₂ on MPh, B-MPh, or N-MPh (averages and standard deviations of inner (α), outer (β), and peripheral (γ) sphere C–C distances in Å, out-of-plane distortion (δ , Å) of the site of substitution, and methylene group wagging angle (ω , °) of the methyldene group) with one ($n = 1$), two ($n = 2$, opposite face, superscripts indicate occupied rings with adsorbate), and six ($n = 6$, model saturation) adsorbate molecules described by H₂ bond centroid (X_{H_2}) and nearest ring centroid (X_i) distances (d_i , Å where i subscript represents ring I, II, or III H₂ is located above), H₂ angle of approach defined by ring centroid(X_i)···H–H (φ , °) ranging from end-on ($\varphi = 180^\circ$) to side-on ($\varphi = 90^\circ$) orientation, tilt with respect to the site of substitution ($X1$) defined by $X1$ ···ring centroid···proximal H (ϕ , °) bond angles, degree of deviation from centeredness of the H–H bond centroid projections to the plane of the ring centroids from the nearest ring centroid (λ , Å), and H–H bond lengths of the adsorbed H₂ molecule.

Adsorbent	LoT	N	inner	outer	peripheral	δ	ω	d_i	φ	ϕ	λ	$\square-\square^a$
MPh	MN15	1 ^I	1.43±0.00	1.42±0.04	1.39±0.04	0.00	176	3.04	167	87	0.05	0.739
		1 ^{II}	1.43±0.00	1.42±0.04	1.39±0.04	0.00	176	3.02	169	87	0.05	0.739
		1 ^{III}	1.43±0.00	1.42±0.04	1.39±0.04	0.00	176	3.02	171	87	0.06	0.739
	MN15	2 ^{II,III}	1.43±0.00	1.42±0.04	1.39±0.04	0.00	176	3.02±0.00	173± 3	87± 0	0.04±0.00	0.739±0.000
	MN15	6	1.43±0.00	1.42±0.04	1.39±0.04	0.00	176	3.02±0.09	140±35	83± 3	0.12±0.04	0.739±0.000
B-MPh	MN15	1 ^I	1.52±0.01	1.42±0.04	1.41±0.04	0.00	172	3.02	143	87	0.11	0.740
		1 ^{II}	1.52±0.01	1.42±0.04	1.41±0.04	0.00	172	3.03	174	88	0.05	0.740
		1 ^{III}	1.52±0.01	1.42±0.04	1.41±0.04	0.00	172	3.04	164	86	0.06	0.740
	MN15	2 ^{II,III}	1.52±0.01	1.42±0.04	1.41±0.04	0.00	172	3.04±0.01	167±10	87± 2	0.05±0.01	0.740±0.000
	MN15	6	1.52±0.01	1.42±0.04	1.41±0.03	0.00	172	3.04±0.02	146±26	88± 3	0.13±0.05	0.740±0.000
N-MPh	MN15	1 ^I	1.41±0.01	1.42±0.040	1.39±0.03	0.01	176	2.83	109	90	0.13	0.740
		1 ^{II}	1.41±0.01	1.42±0.040	1.39±0.03	0.01	177	2.85	108	85	0.21	0.740
		1 ^{III}	1.41±0.01	1.42±0.040	1.39±0.03	0.01	177	2.86	119	88	0.18	0.740
	MN15	2 ^{II,I}	1.41±0.01	1.42±0.040	1.39±0.03	0.01	175	2.84±0.02	104± 1	87±23	0.16±0.07	0.740±0.000
	MN15	6	1.41±0.01	1.42±0.040	1.39±0.03	0.02	175	2.98±0.17	125±37	82± 3	0.15±0.10	0.740±0.000

^a free H–H distance at MN15 level is 0.738 Å

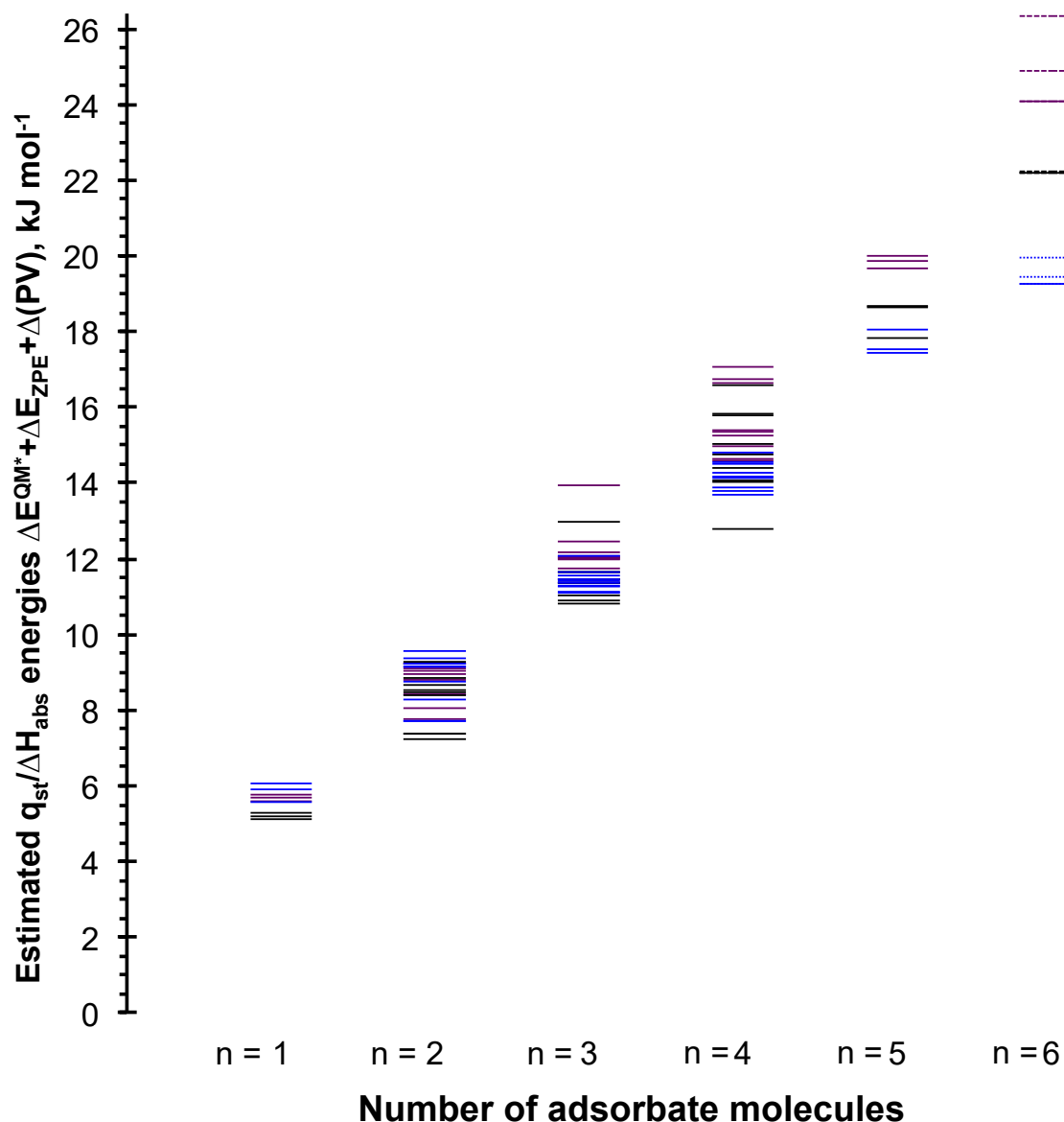


Figure S3: Estimated adsorption energies with BSSE and zero-point energy corrections according to $\Delta E^{QM*} + \Delta E_{ZPE} + \Delta(PV)$ at MN15/6-311++G** level of theory) for all models shown in **Scheme S2**. The dashed lines for the $n = 6$ adsorption models indicate structural isomers obtained by permuting the identity of the central site of substitution, X1, in the X-MPh model from the lowest energy structures represented by the solid lines. The permutation of composition was carried out in order to address potential pitfalls of comparing local as opposed to global potential energy surface minima. All of these permuted structures are higher in energy by at least more than 2.3, 0.1, and 0.7 kJ mol^{-1} for X = B, C, and N when using X = (C or N), (B or N), and (B or C) compositions, respectively.

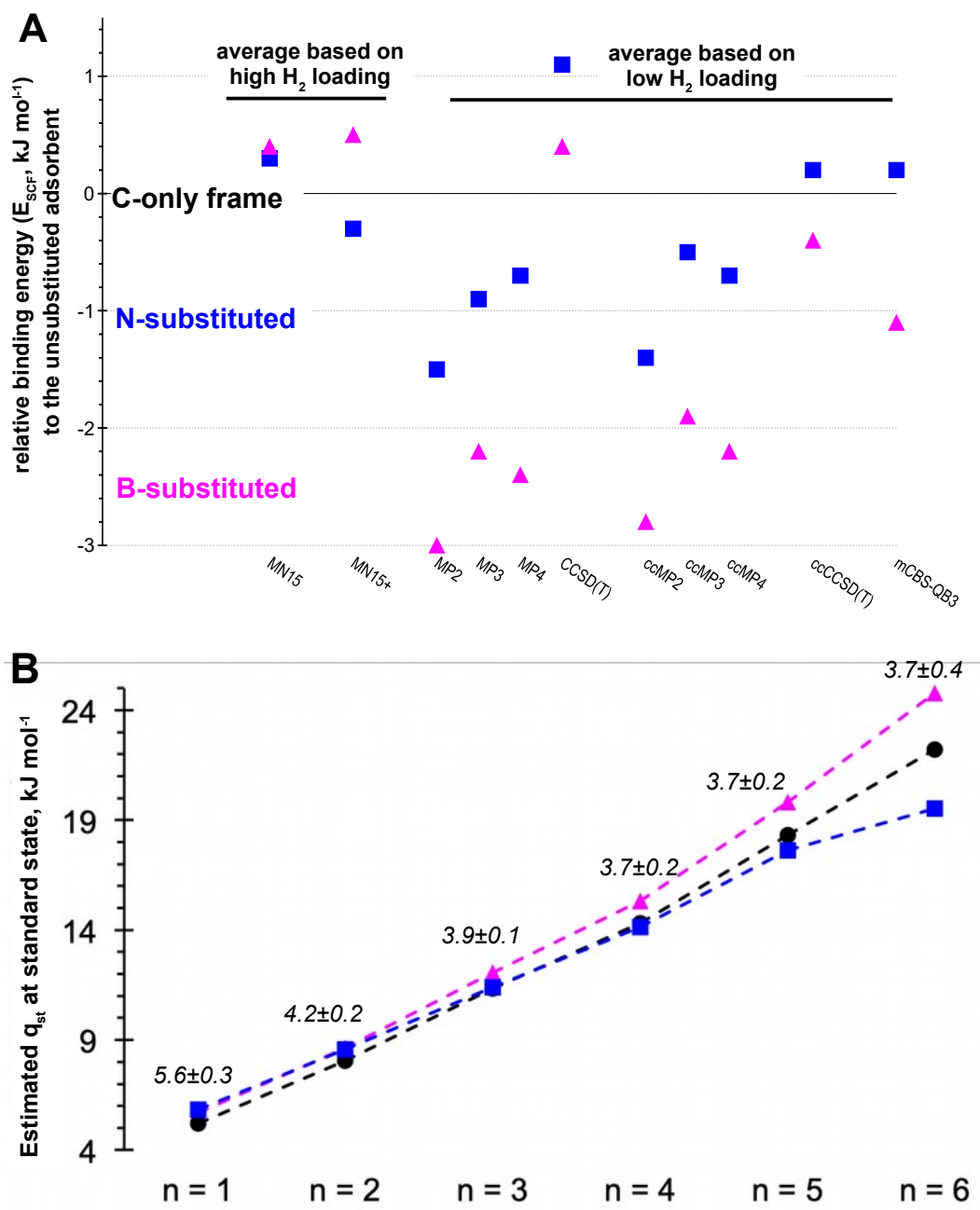


Figure S4: Level of theory dependence of MPH adsorbent/ H_2 adsorbate interaction energies for (Panel A) and Boltzmann weighed dissociation energies at standard state using $\Delta(E^{\text{QM}^*} + E_{\text{ZPE}} + \Delta(\text{PV}))$ formalism from MN15/6-311++G** calculations as a function of surface coverage ($n = 1-6$) for X-MPh $\times n\text{H}_2$ (X = C shown as black circles, X = B as pink triangles, and X = N as blue squares) physisorption models (Panel B; the italicized numbers above data points correspond to average q_{st} values in kJ mol^{-1} per H_2 molecule; the overall per H_2 heat of adsorption was estimated to be $4.1 \pm 0.7 \text{ kJ mol}^{-1}$).

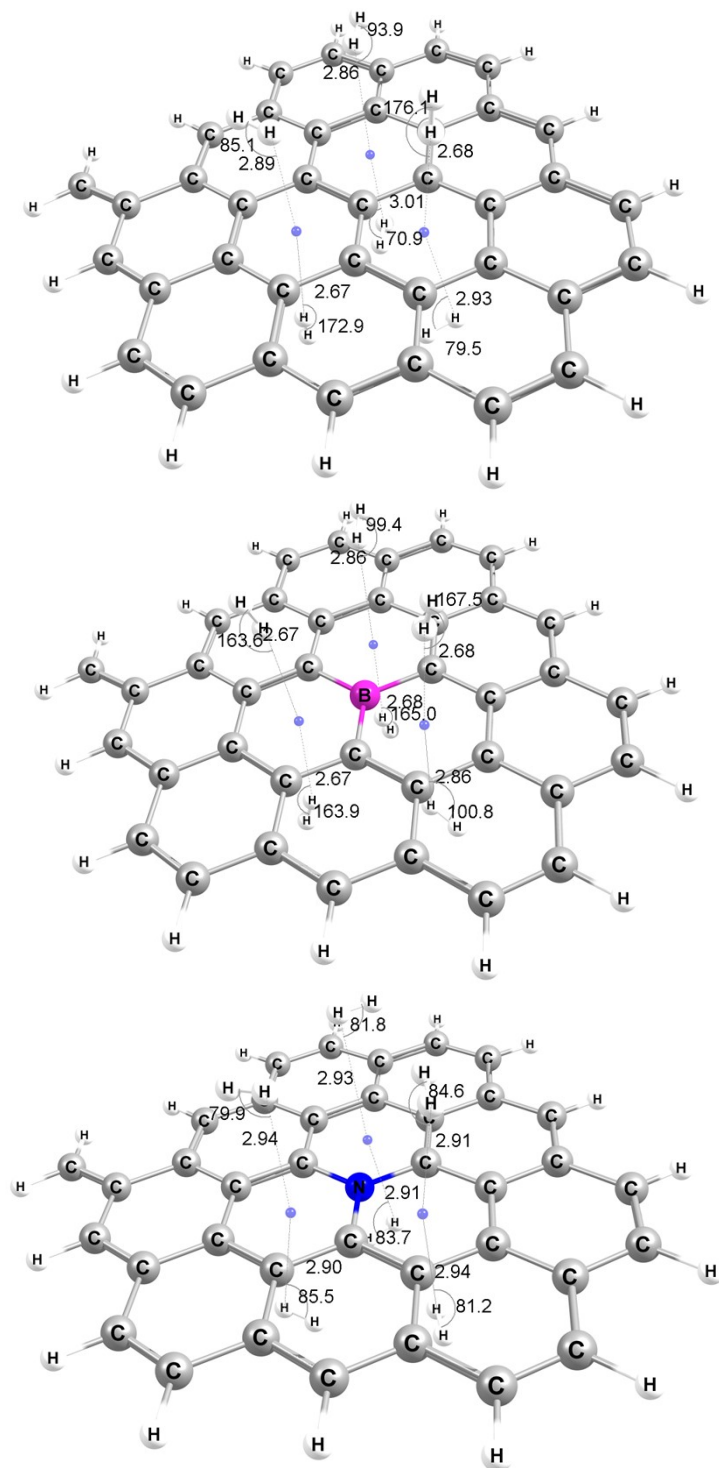


Figure S5: Comparison of optimized models at MN15/6-311++G** level of theory considering perbenzannulated MPh models (X-pbaMPh, X = C, B, or N) with key structural parameters (d_1 and φ) describing the H₂ interactions.

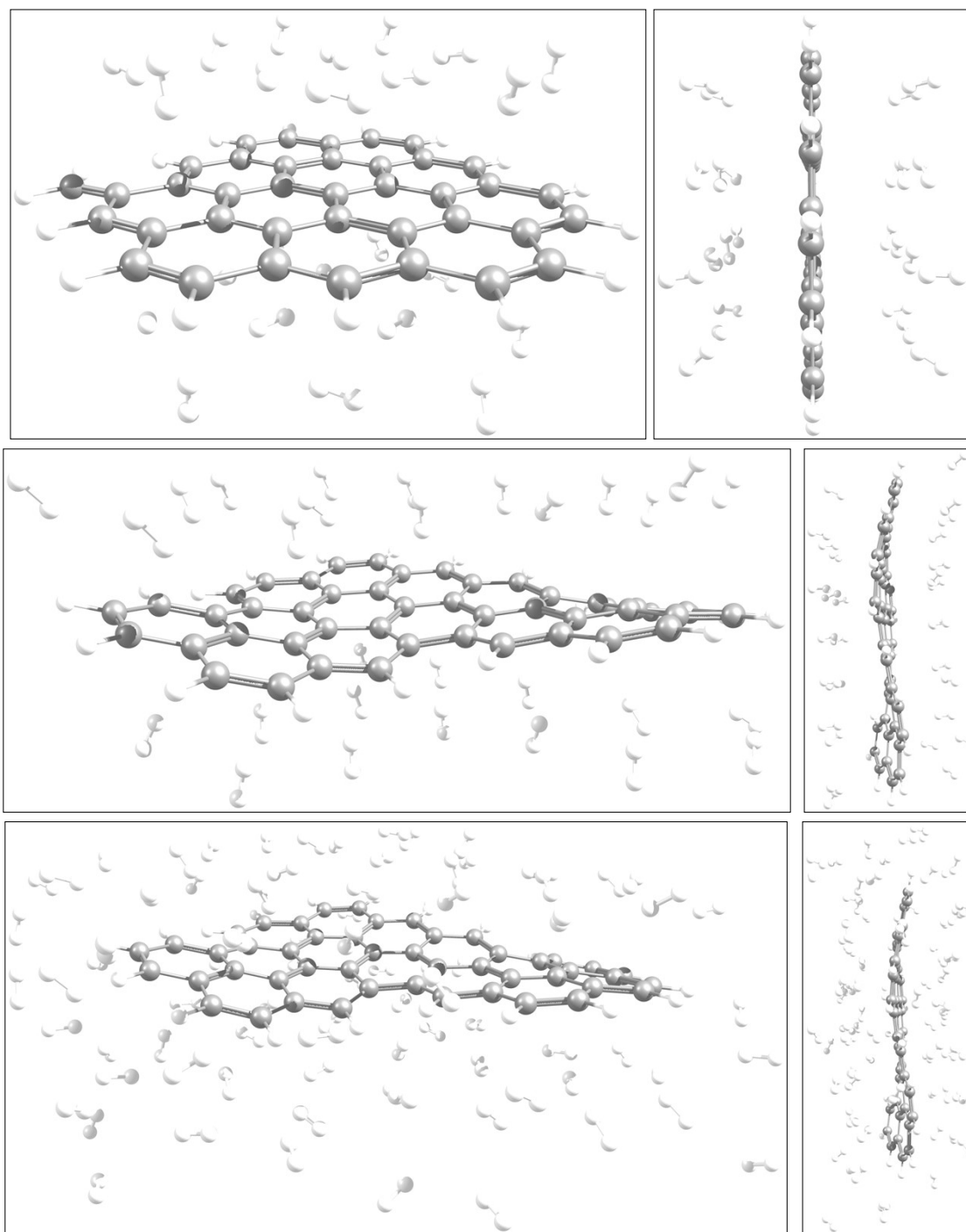


Figure S6: Two views of high H₂ loading adsorption models optimized at MN15/6-311++G** level of theory using the X-pbaMPh adsorbent with 24 adsorbate molecules (top row) and curved blade models (middle and bottom rows) corresponding to low density (15 mol dm⁻³; 30 adsorbates, middle row) and high density (38 mol dm⁻³; 84 adsorbates, bottom row) liquid H₂ environments. The top two models started from approximately co-linear, end-on H₂ arrangements perpendicular to the closed ring with a 2.7 Å ring-centroid-to-proximal H distances, while the lower model was created by soaking the curve blade in liquid H₂.

Table S5: Dissociation energies (in kJ mol^{-1}) for $(\text{adsorbent}) \times n\text{H}_2 \rightarrow \text{adsorbent} + n\text{H}_2$ reactions obtained from MN15/6-311++G** calculations. BSSE stands for basis set superposition error (in kJ mol^{-1}). The structures of the extended models are shown in **Figures S5-S6**. ΔH_{ads} or q_{st} is calculated by using $\Delta E^{\text{QM}^*} + \Delta E_{\text{ZPE}} + \Delta PV$ (see **Figure S8**). Interaction energies (ΔE^{QM^*}) among the adsorbates are -16 and -139 kJ mol^{-1} for 6 and 30 H_2 molecules or -2.6 and -4.6 kJ mol^{-1} per molecule, respectively. B₃ and N₃ prefixes correspond to triple heteroatom substituted models, where the site of substitutions are separated by at least three C atoms.

Adsorbent	n	ΔE^{QM}	BSSE	q_{st} per H_2
pbaMPh	6	57	7	3.3
B-pbaMPh	6	56	8	2.7
N-pbaMPh	6	54	7	2.3
pbaMPh	24	241	15	3.6
B-pbaMPh	24	220	14	3.0
N-pbaMPh	24	231	10	2.5
blade	30	298 or 9.9 per H_2		
B ₃ -blade	30	287 or 9.6 per H_2		
N ₃ -blade	30	295 or 9.8 per H_2		
blade	33 ^a	232 or 7.0 per H_2		
blade	84 ^a	625 or 7.4 per H_2		

^a initial H_2 positions (d_i) and orientations (ϕ) were randomized.

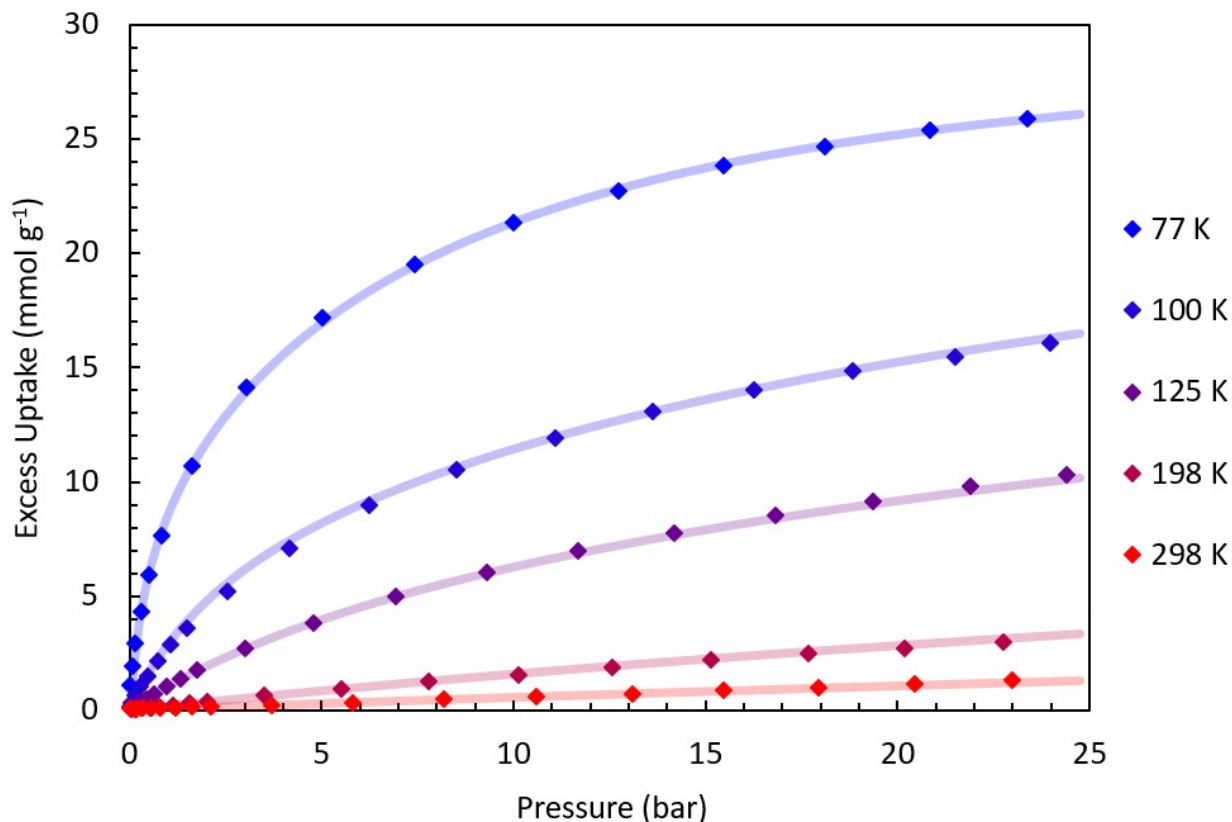


Figure S7. Experimental adsorption isotherms of H₂ on ZTC at 77–298 K, fitted to three models to determine the experimental heat of H₂ adsorption (ΔH_{exp} or q_{st}).

Experimental isosteric heats of H₂ adsorption on ZTC were calculated by fitting the raw experimental adsorption isotherms (excess adsorbed amount as a function of temperature and pressure, Figure S6) to three Langmuir-type models: single-site, dual-site, and Unilan. The best fit was to a dual-site model of the following form:

$$n_e[T,P] = (n_{\text{max}} - \rho_g[T,P] V_a) \left((1 - \alpha) \left(\frac{K_1 P}{1 + K_1 P} \right) + \alpha \left(\frac{K_2 P}{1 + K_2 P} \right) \right)$$

$$K_i = \frac{A_i}{\sqrt{T}} e^{-\left(\frac{E_i}{RT}\right)}$$

The isosteric heat of adsorption (ΔH_{exp} or q_{st}) was then derived analytically by solving the Clapeyron equation, without any requirement that the gas phase be ideal. Details as to this method were previously reported [Ref. 53]. The best-fit parameters are shown in Table S6. The results are in agreement with past work [Ref. 4] up to 30 MPa at 298 K, and hence the isosteric heat is plotted to high coverages comparable to the range investigated computationally in the present work.

Table S6. Best fit values for parameters that describe H₂ adsorption on ZTC at 77–298 K within the framework of a dual-site Langmuir model (DL in **Figure S8**).

Parameter	Symbol	Value	Units
Number of Adsorption Sites	n_{max}	34.2	mmol g ⁻¹
Max Volume of Adsorbed Phase	V_a	0.349	mL g ⁻¹
Fraction of Sites of Type 2	α	0.739	(none)
Pre-Exponential Factor Type 1	A_1	1.36×10 ⁻¹	MPa ⁻¹ K ^½
Binding Energy of Type 1	E_1	4.62	kJ mol ⁻¹
Pre-Exponential Factor Type 2	A_2	1.72×10 ⁻²	MPa ⁻¹ K ^½
Binding Energy of Type 2	E_2	4.05	kJ mol ⁻¹

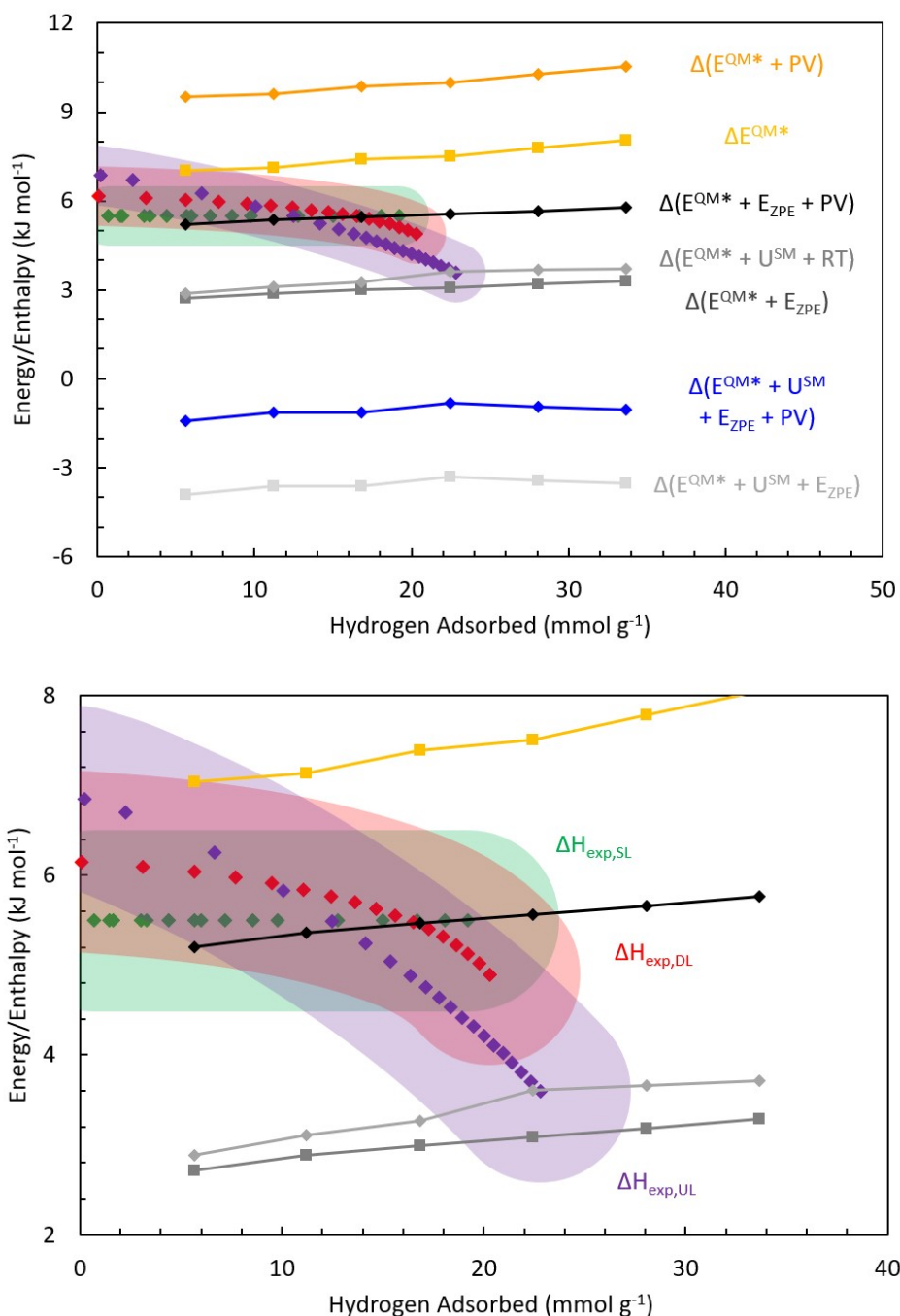


Figure S8. Experimental isosteric heat of H₂ adsorption on ZTC (ΔH_{exp} or q_{st}) as a function of H₂ loading at room temperature, compared to various calculated quantities. USM stands for the thermal energy correction to the internal energy from statistical mechanics. The computationally-derived quantity that most closely matches experiment is the same as in previous work [Ref. 30]: $\Delta H_{ads} \approx \Delta E^{QM*} + \Delta E_{ZPE} + \Delta PV$. Squares represent energies and diamonds represent enthalpies. The width of the transparent regions represents the uncertainty inherent to the experimental method. SL, DL, and UL stand for single-site, double-site, and uniform (“Unilan”) Langmuir models, respectively.